International Journal of Microwave and Wireless Technologies

cambridge.org/mrf

Research Paper

Cite this article: Sarin VP, Vinesh PV, Manoj M, Aanandan CK, Mohanan P, Vasudevan K (2021). Toroidal dipole excitation in cylindrically arranged dogbone metallic inclusions. *International Journal of Microwave and Wireless Technologies* 1–6. https://doi.org/10.1017/S1759078720001683

Received: 26 July 2020
Revised: 2 December 2020
Accepted: 2 December 2020

Key words:
Toroidal dipoles; Multipole scattering; Forward scattering

Author for correspondence:
V. P. Sarin, E-mail: sarincrema@gmail.com

Toroidal dipole excitation in cylindrically arranged dogbone metallic inclusions

V. P. Sarin[1], P. V. Vinesh[1,2], M. Manoj[2], C. K. Aanandan[2], P. Mohanan[2] and K. Vasudevan[2]

[1]Department of Electronics, Government College Chittur, Palakkad, Kerala, India and [2]Centre for Research in Electromagnetics and Antennas, Cochin University of Science and Technology, Kochi, Kerala, India

Abstract

A significant excitation of toroidal moments in cylindrically arranged dogbone metallic inclusions is validated and presented in this paper. The antiparallel poloidal currents excited on the front and back faces of the proposed cylindrical dogbone inclusions create strong magnetic field confinement at the center generating intense toroidal moments on the structure. The significant excitation of toroidal dipole moment causes an improvement in the scattering cross-section from the resonant system. The resonant mechanism is analyzed using the multipole scattering theory, and we used the scattering measurement techniques to characterize the structure experimentally in the microwave regime.

Introduction

Plane-wave scattering from metamaterials exhibiting toroidal dipole moments is a rapidly growing research area. Toroidal multipole moment is the higher-order multipole in the multipole scattering expansion. When the object size approaches the order of incident wavelength, then multipole theory shows the presence of toroidal moments. For sub-wavelength particles, only the first-order electric and magnetic dipole moments will be excited. Kerker and coworkers pointed out that when the electric and magnetic moments on these sub-wavelength inclusions are equal in magnitude and oscillating in phase, then forward scattering is observed [1, 2]. An out-of-phase oscillation reduces the scattering cross-section of the object [3]. The lack of natural magnetic materials remained a bottleneck until Pendry *et al.* demonstrated the first practical realization of artificial magnetism using the so-called split-ring resonator array [4]. The practical applications of such metamaterials are listed in various review reports [5].

Recently, toroidal dipole excitation in metamaterials has gained considerable interest due to their promising electromagnetic behaviors such as high near-field energy localization, high Q-factor, etc. Toroidal moments are created by the poloidal or the axial current distributions excited on the composite [6]. Classical electromagnetic theory neglects the excitation of this higher-order moment [7], and Zel'dovich first reported their excitation in nuclear systems [8]. Specially designed asymmetric configurations of split-ring resonators and stacked structures show toroidal moments [9–12]. Dielectric resonator-based techniques are also employed to overcome losses due to conduction currents [13]. Toroidal moments are created in the visible and ultraviolet range, using silicon-based dielectric materials [14, 15]. Recently, scattering from composite metamaterial structures is manipulated using toroidal dipole moments. Toroidal dipole excitation also ensures coherent forward scattering [16, 17]. The parallel excitation of overlapped toroidal and electric dipole moments is an anapole, and the resulting structure is invisible to a radar located at the far-field [18, 19]. Recently, toroidal metamaterial with tunable resonant behavior is observed in the THz range [20].

The specialty of dogbone metamaterials is that its dimensions are the order of the operation wavelength at resonance. Hence, toroidal dipole moments could be excited in specialized cylindrical configurations of dogbone structures. One such design is the cylindrically arranged dogbone elements around a metallic target [16] and is a modification of the authors' cylindrical cloaking structure [21]. The authors also detected a Fano-like resonance profile by exciting strong magnetic resonance to create an electromagnetic invisibility cloaking scheme in a separate spectral window devoid of toroidal excitation [22]. This paper proposes a modified dogbone-based cylindrical structure that shows a significant improvement in toroidal excitation. The authors have used full-wave electromagnetic simulations for optimization, and backscattering from the design is measured using PNA E8362B network analyzer.

The geometry of the structure

The unit-cell structure is a modification of our previous work [16], and the main difference is that it is devoid of the enclosed metallic cylindrical target, as shown in Fig. 1. All the

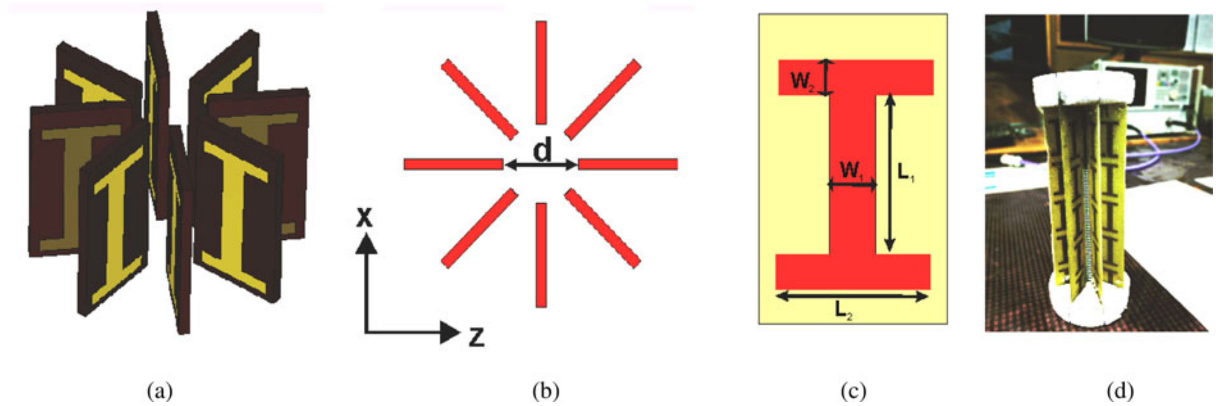

Fig. 1. Description of the structure under study. (a) Formation of the unit cell, (b) top view, (c) geometrical specifications ($L_1 = 18$ mm, $L_2 = 12$ mm, $W_1 = 4$ mm, $W_2 = 2$ mm, $d = 14.5$ mm), and (d) photograph of the fabricated structure.

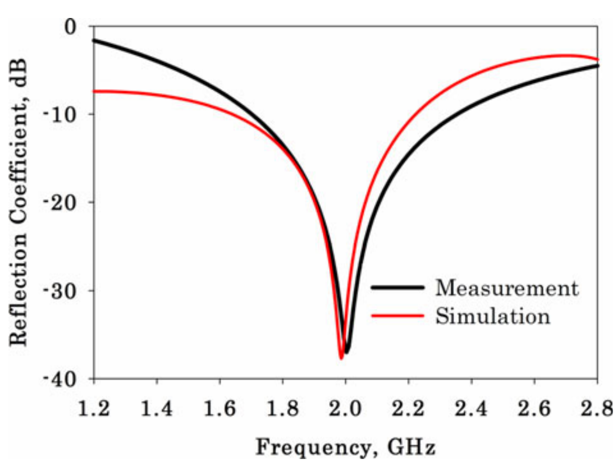

Fig. 2. Reflection coefficient of the proposed structure.

other parameters remain the same. Eight dogbone metallic elements, printed on a substrate of dielectric constant 4.4 and height 1.6 mm, are arranged in a coaxial fashion, as depicted in Fig. 1(a). Figure 1(b) shows the top view of the structure. The inner diameter d is selected to be 14.5 mm. Figure 1(c) illustrates the unit-cell dimensions. We have used photolithographic etching techniques for fabrication, and the engraved copper thickness is 35 µm. The final full design used for measurement utilizes five such unit cells arranged vertically, as shown in Fig. 1(d).

Simulation and measurement studies

We have used CST Microwave Studio for full-wave simulation studies of the structure. For that, a plane wave with polarization along y-axis is incident on the full structure shown in Fig. 1(d). Reflectance from the design is measured using a monostatic scattering measurement setup for normal incidence. For that, two ultra wideband antennas, with an azimuth offset of 5°, are mounted on a turntable assembly. We placed a metallic cylinder at the turntable assembly center for performing a THRU calibration. To avoid possible multipath clutters, proper time gating is applied to receive reflections only from the target. Replacing the reference target with the studied structure gives the design's reflectance, as depicted in Fig. 2, and is well matched. The observed resonance is around 2 GHz, and it indicates strong back-scattering suppression at resonance.

The far-field scattering characteristics are studied using full-wave simulations and shown in Fig. 3. The scattering cross-section thus obtained for the structure compared with a metallic plane target is shown in Fig. 3(a). Around resonance, the design shows tremendous enhancement in scattered power as that of the bare metallic cylinder. Figures 3(b) and 3(c) compare the 3D scattering characteristics of both these structures. The cylindrical reference target shows omni-directional scattering, whereas the proposed structure scatters more power along the forward direction. Figures 3(d) and 3(e) represent the scattering patterns along the azimuth and elevation planes. It shows coherent forward scattering in both these planes. The 3 dB beamwidth is 57.6° and 111°, respectively, in these planes.

Multipole scattering theory helps to study the scattering contribution from different multipoles [9]. The power scattered from different multipoles is found by extracting the surface current distributions from the structure and then performing spatial integration as

$$P = \frac{1}{i\omega}\int Jd^3r, \tag{1}$$

$$M = \frac{1}{2c}\int (\vec{r}XJ)d^3r, \tag{2}$$

$$T = \frac{1}{10c}\int [(\vec{r}.J) - 2r^2J]d^3r. \tag{3}$$

The results of these computations give scattered power from different multipoles. In the above equations, P and M represent the lower order electric, magnetic dipole moments, T represents the higher-order Toroidal dipole moment, c is the velocity of light in vacuum, $\vec{r}$ is the displacement vector from the origin, ω is the angular frequency, and J is the surface current density.

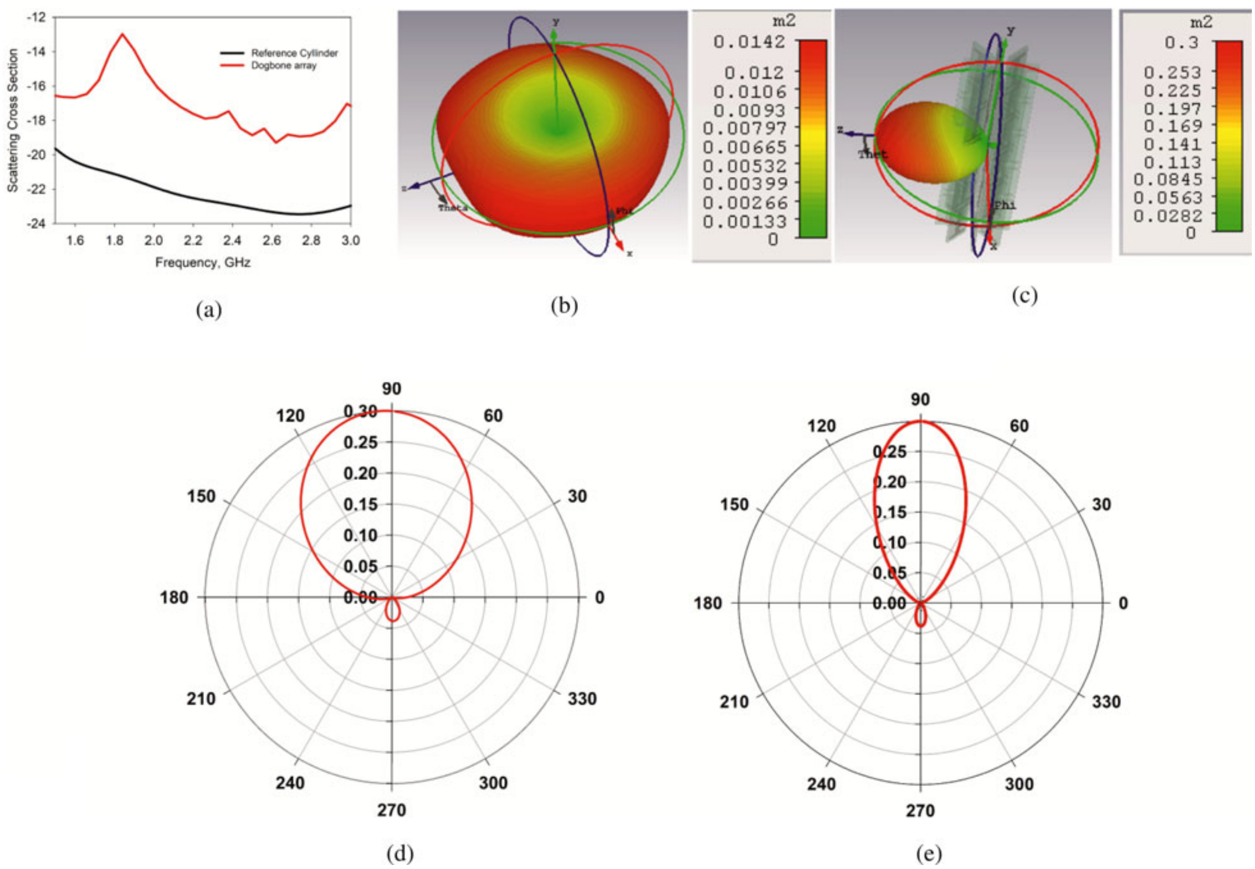

Fig. 3. Results of scattering studies performed. (a) Scattering cross-sections, (b) 3D scattering pattern of a bare metallic cylinder, (c) 3D scattering pattern of the proposed dogbone array, (d) azimuth plane RCS patterns, and (e) elevation plane RCS patterns.

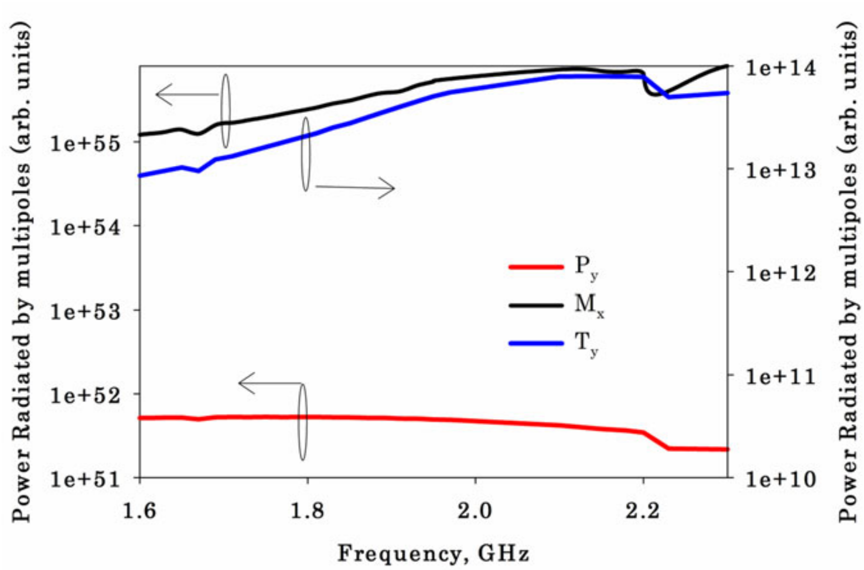

Fig. 4. Radiation contribution from different multipoles.

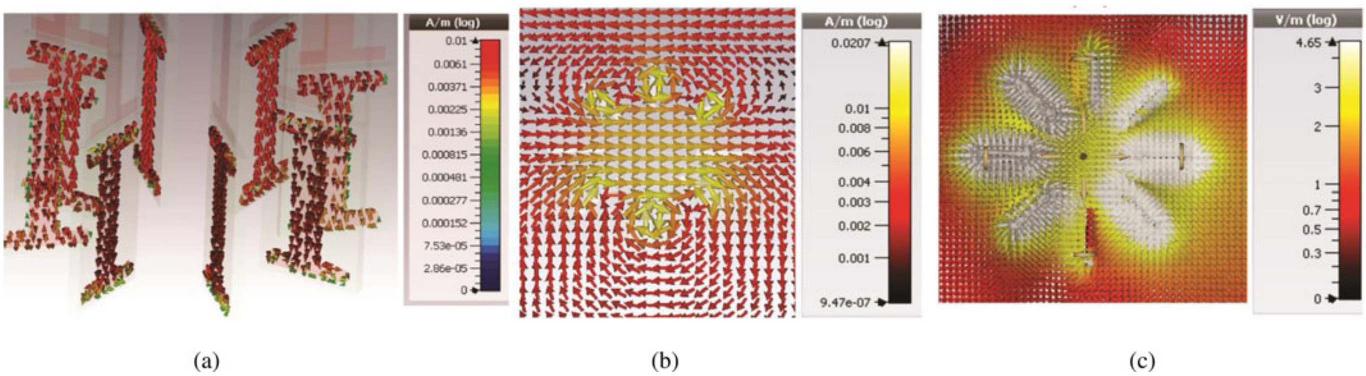

Fig. 5. Resonant field distributions on the structure. (a) Computed current distribution, (b) cross-sectional view of the magnetic field, and (c) electric field distributions.

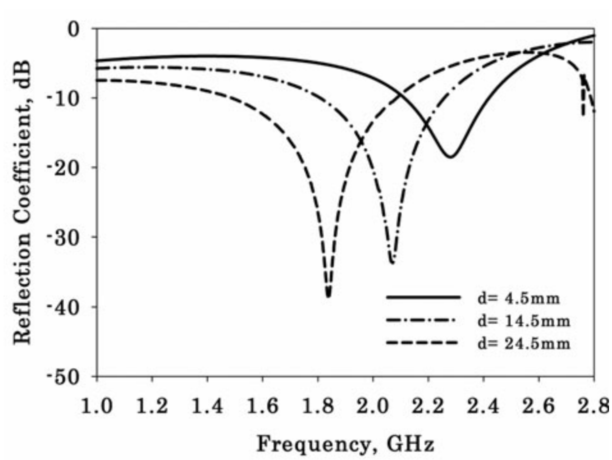

Fig. 6. Effect of inner diameter on reflection coefficient for normal incidence.

Figure 4 illustrates the radiated power contribution from the P_y (electric), M_x (magnetic), and T_y (toroidal) moments. One could see here that power released from the magnetic dipole moment (black line) exceeds that from electric dipole moment P_y (redline) throughout the entire bandwidth under consideration. The power radiated from the magnetic moment M_x is 7000 times higher than that from the electric moment P_y at resonance. The radiated power contribution from the toroidal moment T_y is also indicated in the figure using a solid blueline. We could observe that power radiated from the toroidal moment is significantly high from this structure compared to our previous design [16]. The excitation of toroidal mode is responsible for coherent forward scattering from it at normal incidence.

The cross-sectional magnetic field distributions are useful in studying the excitation of toroidal moments on the structure. Figure 5 shows the resonant surface current and the cross-sectional magnetic fields excited on the cell. Figure 5(a) confirms that the surface currents excited on the structure's input entrance and output faces are out of phase. These antiparallel current distributions create out-of-phase magnetic moments, creating strong in-phase magnetic field distribution at the center of the structure, causing toroidal moments T_y, as depicted in Fig. 5(b). The out-of-phase circulation of surface currents on the structure's input and output faces cancels the contribution of electric dipole moment P_y on far-field radiation. The unit-cell system will act as an efficient dielectric sensor because the enhanced magnetic energy density at the center of the structure enhances the sensor's sensitivity due to toroidal excitation. Figure 5(c) illustrates the computed cross-sectional electric field distribution at resonance. The electric field is concentrated on the top and bottom boundaries of the dogbone particle and is found minimum at the center where the magnetic field is maximum.

To study the effect of the inner diameter on reflection coefficient, we performed a detailed parametric analysis because this inner diameter significantly affects the coupling between dogbone metal strips. Figure 6 illustrates the effect of variation on reflection coefficient for normal incidence. An increase in the diameter of the cell redshifts the resonant frequency. The inner diameter increases the magnetic resonant patch length due to the significant increase in displacement current channel. Moreover, this change causes an increase in reflection from the structure, and the system becomes more inductive due to the enhancement in the mutual inductance between consecutive dogbone elements.

We performed the scattering measurements inside an anechoic chamber, and Fig. 7 illustrates these results. For that, the same methodology adopted for cloaking measurements is used [21]. Figure 7(a) shows the monostatic backscattered power from the structure for normal incidence. In this measurement, we rotated the design in the azimuth plane and recorded the received power. Measurements show that more than −20 dB reduction in backscattered power is observed for all the azimuth angles at resonance. The polar plot of monostatic backscattered power at resonance shown in Fig. 7(b) verifies this observation. Figure 7(c) illustrates the measured bistatic radar cross section (RCS). A significant reduction in backscattered power better than −7.1 dB is observed in comparison with the reference cylinder.

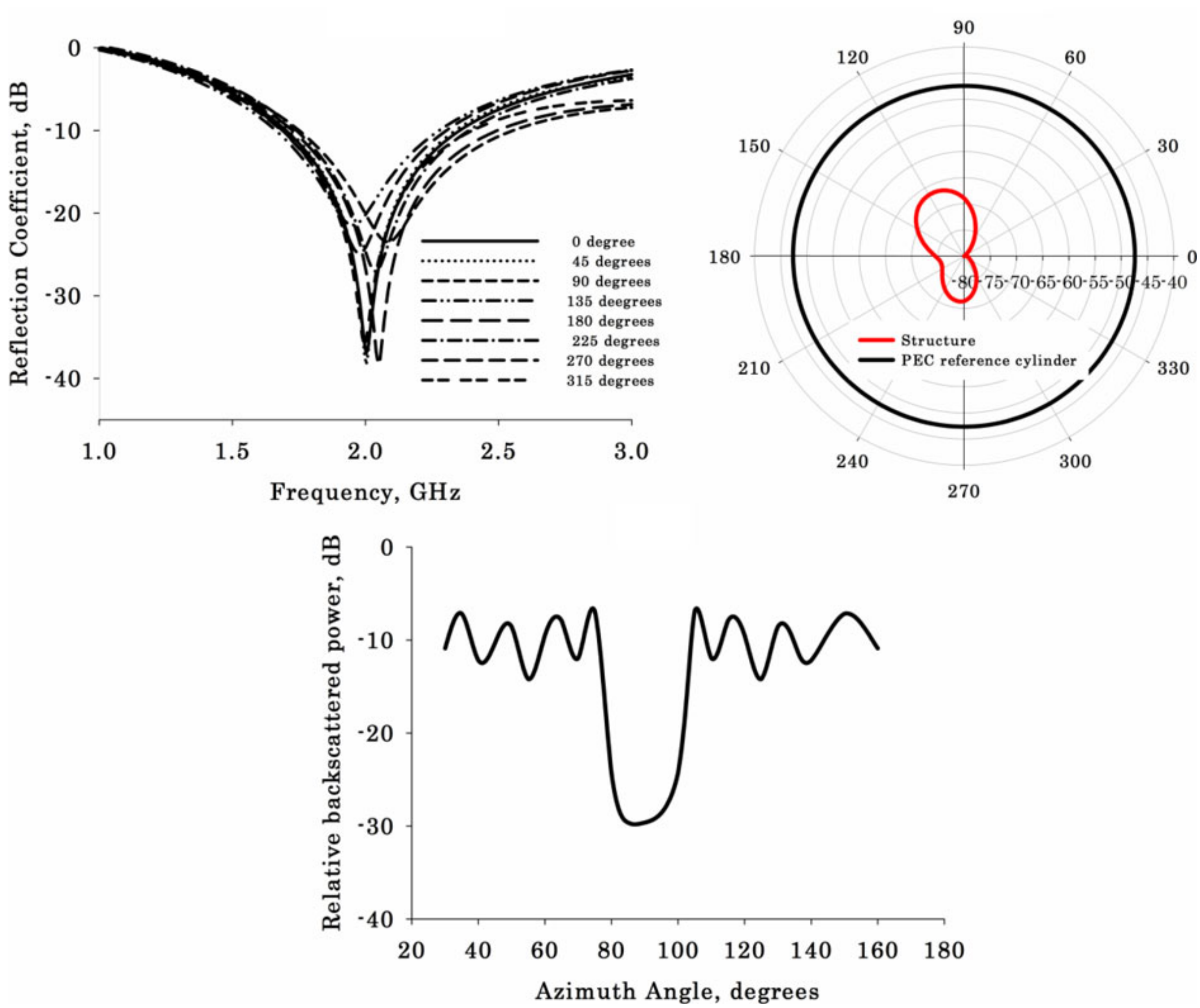

Fig. 7. Results of RCS measurements. (a) Monostatic measurements, (b) polar plot of monostatic backscattered power, and (c) bistatic measurements.

Conclusions

This paper showed the physical excitation of toroidal moments on cylindrically arranged metallic dogbone inclusions in the microwave regime. The anti-phase magnetic moments excited on the structure's input and output faces create strongly enhanced magnetic field confinement at the center, yielding strongly enhanced toroidal moment. Multipole scattering reveals that significant excitation of magnetic and toroidal dipoles enhances forward scattering from the structure at resonance. The results are verified using full-wave electromagnetic simulations and are physically validated in experiments using radar cross-section measurements.

Acknowledgements. The research work is supported by the funding from the Science and Engineering Research Board (SERB), Department of Science and Technology (DST), Govt. of India for the major research project ECR/2017/002204.

References

1. **Kerker M, Wang DS, Chew H and Cooke DD** (1980) Does Lorentz-Mie scattering theory for active particles leads to a paradox? *Applied Optics* **19**, 1231–1232.
2. **Kerker M, Wang DS and Giles L** (1983) Electromagnetic scattering by magnetic spheres. *Journal of the Optical Society of America* **73**, 765–767.
3. **Kerker M** (1975) Invisible bodies. *Journal of the Optical Society of America* **65**, 376–379.
4. **Pendry JB, Holden AJ, Robbins DJ and Stewart WJ** (1999) Magnetism from conductors and enhanced nonlinear phenomena. *IEEE Transactions on Microwave Theory and Techniques* **47**, 2075–2084.
5. **Ziolkowski RW and Engheta N** (2020) Metamaterials: two decades past and into their electromagnetics future and beyond. *IEEE Transactions on Antennas and Propagation* **63**, 1232–1237.
6. **Afanasiev GN and Stepanovsky YP** (1995) The electromagnetic field of elementary time-dependent toroidal sources. *Journal of Physics A: Mathematical and General* **28**, 4565.
7. **Jackson JD** (1999) *Classical Electrodynamics*, 3rd Edn. Hoboken: Wiley.
8. **Zel'dovich IB** (1958) The relation between decay asymmetry and dipole moment of elementary particles. *Journal of Experimental and Theoretical Physics* **6**, 1184.
9. **Kaelberer T, Fedotov VA, Papasimakis N, Tsai DP and Zheludev NI** (2010) Toroidal dipolar response in a metamaterial. *Science (New York, N.Y.)* **330**, 1510–1512.
10. **Gupta M, Savinov V, Xu N, Cong L, Dayal G, Wang S, Zhang W, Zheludev NI and Singh R** (2016) Sharp toroidal resonances in planar terahertz metasurfaces. *Advanced Materials* **28**, 8206–8211.
11. **Gupta M and Singh R** (2016) Toroidal versus Fano resonances in high Q planar THz metamaterials. *Advanced Optical Materials* **4**, 1–7; 201600553.
12. **Fan Y, Wei Z, Li H, Chen H and Soukoulis CM** (2013) Low-loss and high-Q planar metamaterial with toroidal moment. *Physical Review B* **87**, 115417.

13. **Tasolamprou AC, Tsilipakos O, Kafesaki M, Soukoulis CM and Economou EN** (2016) Toroidal eigenmodes in all-dielectric metamolecules. *Physical Review B* **94**, 205433.
14. **Zografopoulos DC, Ferraro A, Algorri JF, Martín-Mateos P, García-Cámara B, Moreno-Oyervides A, Krozer V, Acedo P, Vergaz R, Sánchez-Pena JM and Beccherelli R** (2019) All-dielectric silicon metasurface with strong sub-tera hertz toroidal dipole resonance. *Advanced Optical Materials* **7**, 1900777.
15. **Kuznetsov AI, Miroshnichenko AE, Brongersma ML, Kivshar YS and Luk'yanchuk B** (2016) Optically resonant dielectric nanostructures. *Science (New York, N.Y.)* **354**, aag2472.
16. **Sarin VP, Vinesh PV, Manoj M, Aanandan CK, Mohanan P and Vasudevan K** (2020) Toroidal dipole-induced coherent forward scattering from a miniaturized cloaking structure. *Applied Physics A: Materials Science & Processing* **126**, 1–8.
17. **Terekhov PD, Baryshnikova KV, Shalin AS, Karabchevsky A and Evlyukhin AB** (2017) Toroidal dipole associated resonant forward scattering of light by Silicon nanoparticles. Progress In Electromagnetics Research Symposium – Spring (PIERS).
18. **Miroshnichenko AE, Evlyukhin AB, Yu YF, Bakker RM, Chipouline A, Kuznetsov AI, Luk'yanchuk B, Chichkov BN and Kivshar YS** (2015) Nonradiating anapole modes in dielectric nanoparticles. *Nature Communications* **6**, 8069.
19. **Nemkov NA, Stenishchev IV and Basharin AA** (2017) Nontrivial nonradiating all-dielectric anapole. *Nature Scientific Reports* **7**, 1064.
20. **Song Z, Deng Y, Zhou Y and Liu Z** (2019) Terahertz toroidal metamaterial with tunable properties. *Optics Express* **27**, 5792–5797.
21. **Sarin VP, Jayakrishnan MP, Vinesh PV, Aanandan CK, Mohanan P and Vasudevan K** (2017) An experimental realization of cylindrical cloaking using dogbone metamaterials. *Canadian Journal of Physics* **95**, 927–932.
22. **Pushpakaran SV, Vinesh PV, Manoj M, Aanandan C, Mohanan P and Kesavath V** (2020) Demonstration of Fano resonance-based miniaturized cylindrical cloaking scheme. *Applied Physics A: Materials Science & Processing* **126**, 1–7.

V. P. Sarin received his M.Sc. degree in Applied Electronics in 2006 and the Ph.D. degree in Microwave Electronics from the Cochin University of Science and Technology, Kerala, India, in 2012. He is currently an Assistant Professor in the Department of Electronics, Government College Chittur, Palakkad, Kerala. His main research interests are metamaterials, microwave antennas, and FDTD techniques.

P. V. Vinesh received the B.Sc. degree in Electronics from the University of Kannur, India, and the M.Sc. degree in Electronics from the MES College Erumely, Kottayam, India, in 2004 and 2006, respectively. He is currently working toward the Ph.D. degree at the Cochin University of Science and Technology (CUSAT), Cochin, India. His research interests include designing planar inverted F antennas, loop antennas, multiband antennas, etc.

M. Manoj received his M.Sc. in Electronics from the Cochin University of Science and Technology, Kerala, India, in 2015 and currently pursuing Ph.D. at the Centre for Research in Electromagnetics and Antennas. He was awarded the Junior Research Fellowship by the University Grants Commission in 2014 and had been working at the Cochin University of Science and Technology since 2015. His current research interests include electrically small antennas, RFID tags, and antennas for biomedical applications.

C. K. Aanandan was born in India. He received the M.Sc. and Ph.D. degrees from the Cochin University of Science and Technology (CUSAT), Cochin, India, in 1981 and 1987, respectively. Currently, he is a Professor in the Department of Electronics, CUSAT. From 1997 to 1998, he worked at the Centro Studi Propagazione E Antenne, Consiglio Nazionale Delle Ricerche, Torino, Italy, under the TRIL program of the International Centre for Theoretical Physics (ICTP). His research interests include microstrip antennas, radar cross-section studies, and frequency-selective surfaces.

P. Mohanan was born in India. He received the Ph.D. degree in Microwave Antennas from the Cochin University of Science and Technology (CUSAT), Cochin, India, in 1985. Previously, he worked as an Engineer at the Antenna Research and Development Laboratory, Bharat Electronics, Ghaziabad, India. Currently, he is a Professor in the Department of Electronics, CUSAT. He has published more than 100 refereed journal papers and numerous conference articles. He also holds several patents in the areas of antennas and material science. His research areas include microstrip antennas, dielectric resonator antennas, superconducting microwave antennas, reduction of radar cross-sections, and polarization agile antennas.

K. Vasudevan (SM'84) was born in India. He received the M.Sc. degree in Physics from Calicut University, Kerala, India, and the Ph.D. degree from Cochin University, Cochin, India, in 1976 and 1982, respectively. From 1980 to 1984, he worked at St. Alberts' College Ernakulam, Kerala, India. In 1985, he joined the Electronics Department of CUSAT, where he is currently the Emeritus Professor. His research interests include microstrip antennas, leaky wave antennas, and radar cross-section studies. Dr. Vasudevan is a Fellow of the Institution of Electronics and Telecommunication Engineers (India).

Applied Physics A (2020) 126:566
https://doi.org/10.1007/s00339-020-03757-2

Applied Physics A
Materials Science & Processing

Check for updates

Demonstration of Fano resonance-based miniaturized cylindrical cloaking scheme

Sarin V. Pushpakaran[1] · P. V. Vinesh[1] · M. Manoj[2] · Chandroth Aanandan[2] · P. Mohanan[2] · Vasudevan Kesavath[2]

Received: 28 January 2020 / Accepted: 24 June 2020

Abstract

An experimental realization of a magnetic Fano-like resonance-based cylindrical cloaking scheme in the microwave frequency regime is presented in this paper. Fano-like resonance is excited by the coupling between the background electric dipole mode and the dark magnetic resonant mode in the composite. The excitation of Fano interference patterns significantly reduces scattering from the composite at resonance in the microwave regime and hence the target becomes undetectable from backscattering measurements. Multipolar scattering theory has been used to clarify the excitation of this Fano resonance and the designed cloak is characterized using monostatic and bistatic scattering measurements inside an anechoic chamber.

Keywords Electromagnetic cloaking · Fano resonance · Dogbone metamaterials · Toroidal dipoles

1 Introduction

Electromagnetic scattering reduction from subwavelength structured metallic and dielectric targets is a challenging research topic over the decade. Scattering studies of magneto dielectrics have attracted a wide interest in plasmonics. M. Kerker pointed out some unusual scattering characteristics from magneto dielectrics with specific electromagnetic parameters of spheres and this conclusion is popularly known as Kerker's paradox [1]. When an electromagnetic wave impinges on arrays of subwavelength inclusions, electric and magnetic dipoles will be created on these composites. An equal magnitude in-phase excitation of electric and magnetic moments on the composite exhibits coherent forward scattering and acts like a Huygens's source [2]. An out of phase oscillation between them results in destructive interference resulting in scattering suppression which finds application in electromagnetic cloaking [3]. The invention of metamaterials boosted the research on electromagnetic cloaking due to their unusual material parameters under plane wave excitation. J.B Pendry practically proposed the first cloaking structure using a cylindrical array of specially designed split ring resonator array [4]. An alternate technique is to use a plasmonic cover over the dielectric target to be cloaked [5, 6]. The negative permittivity offered by the outer layer effectively suppresses scattering from the dielectric target. Plasmonic cloaking could be effectively used to cloak a dipole antenna from its surroundings without deteriorating its reception characteristics [7]. But when the size of the target increases, there would be acute scattering from higher-order multipoles in a plasmonic cloak and to overcome this disadvantage mantle cloaking has been proposed [8–11]. In mantle cloaking, a frequency selective surface with suitable surface reactance is selected to reduce scattering from the target. The disadvantage of the above-listed cloaking techniques is that the bandwidth is restricted. Due to practical difficulties associated with the fabrication of metamaterials with extreme parameters, the practical demonstration of a perfect three-dimensional electromagnetic cloaking scheme is still a challenging task. This difficulty is somehow alleviated in Fano interference-based scattering reduction techniques. Fano resonances were initially observed in atomic systems and quantum mechanical systems and shows asymmetric line spectrum [12, 13]. Fano-like resonance, observed in asymmetric configurations, is arising due to the co-existence of a superradiant bright mode and a sub-radiant dark mode

✉ Sarin V. Pushpakaran
sarincrema@gmail.com

1 Department of Electronics, Government College Chittur, Palakkad, Kerala 678104, India

2 Centre for Research in Electromagnetics and Antennas, Cochin University of Science and Technology, Cochin, Kerala 682022, India

[14]. The bright mode usually constitutes an electric dipole resonance and it represents the background mode of the continuum. The weakly radiating dark mode is the anti-parallel currents representing the magnetic resonant modes of the composite. Destructive interference between these modes modifies the scattering contribution from the composite and hence shows a dip in the extinction cross-section [15–17]. Due to suppression of scattering from the electric dipole resonance, Fano resonance-based systems are successfully implemented for the creation of plasmonic magnetic metamaterials [18–20].

In [21], the authors proposed a cylindrical cloaking enclosure for scattering reduction from a metallic cylinder using dogbone inclusions. Dogbone metamaterial exhibits both electric and magnetic resonances and if these resonances occupy the same spectral regime, then the negative refractive index is achieved [22]. The induced electric and magnetic polarizability could be controlled by varying the structural parameters of the dogbone unit cell. They could also be used for reactive to propagation conversion resulting in enhanced radiation performance of a dipole antenna [23]. We have recently observed toroidal dipole mode in a miniaturized version of the dogbone based cloaking structure [24]. The excitation of toroidal moments significantly enhances forward scattering from this structure. In this paper, we are revisiting the same miniaturized structure, in which the destructed toroidal dipole mode in a different spectral window enables a significant reduction of Scattering Cross Section of the structure for normal incidence. The excitation of magnetic Fano-like resonance in the composite creates strong in-phase magnetic dipole moments in the structure thereby destructing toroidal dipole excitation. The results are verified using full-wave electromagnetic simulation and are subsequently validated in experiments with Monostatic and bistatic scattering measurements using PNA E8362B network analyzer.

2 The geometry of the structure

The unit cell of the proposed Fano-like resonance-based miniaturized cloaking structure is shown in Fig. 1. The structure remains the same as that of our previous work [24]. The radius of the hollow metallic cylinder is $r = 5$ mm. It serves as the target under consideration and its length is selected to be 160 mm. A total of eight dogbone metallic elements are arranged around the cylinder as shown in Fig. 1a. The dimensions of the dogbone elements are indicated in Fig. 1b. Standard FR-4 epoxy substrate with relative permittivity 4.4 and thickness 1.6 mm is used for the fabrication of these elements. The engraved metallic thickness is 35 µm. The final structure constitutes five such vertically arranged cells along *Z*-direction and its photograph is shown in Fig. 1c. The geometric parameters of the dogbone metallization are $L_1 = 18$ mm, $L_2 = 12$ mm, $W_1 = 4$ mm and $W_2 = 2$ mm. The separation between the target and the dogbone element is made uniform and is given by $S = 2.5$ mm.

2.1 Results and discussions

Simulation studies have been performed on the cloaking structure using Full-Wave Electromagnetic simulations with CST Microwave Studio. The full structure is illuminated with a plane wave with the electric field polarized along the cylinder axis. Scattering properties of the cloaked and uncloaked targets are illustrated in Fig. 2. Figure 2a

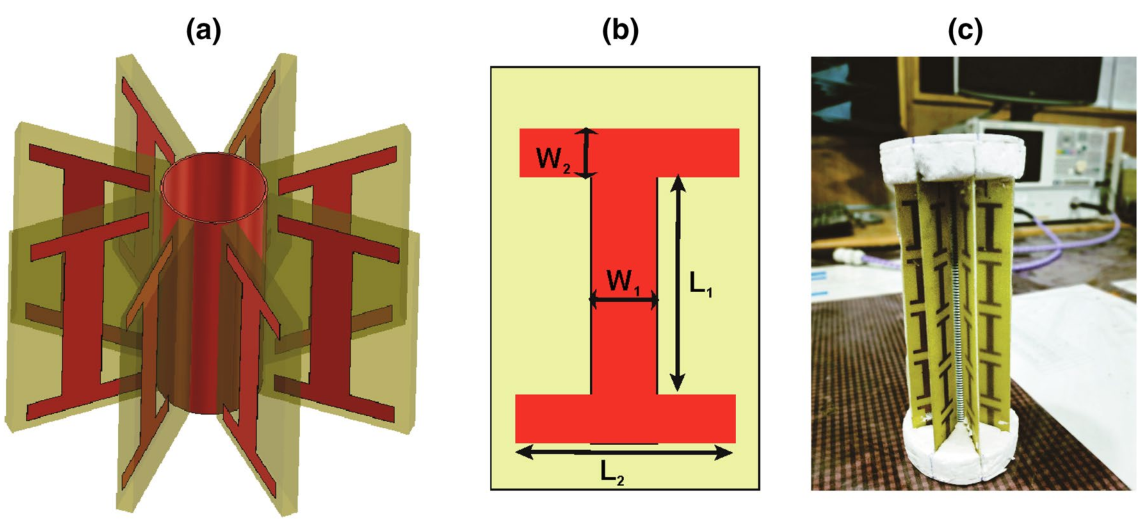

Fig. 1 Geometry of the cloaking scheme **a** construction of the unit cell and **b** geometrical specifications of dogbone metallization and **c** photograph of the fabricated cloak

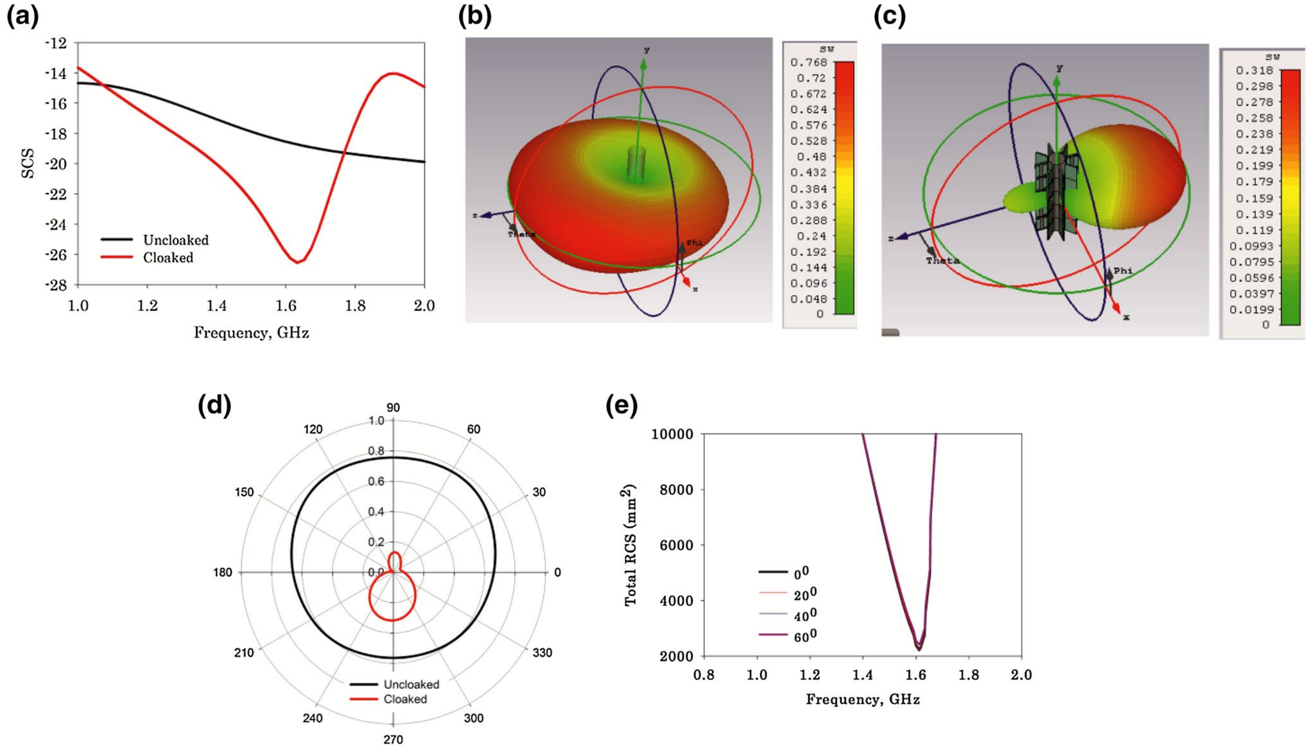

Fig. 2 Scattering characterization of the cloaked and uncloaked targets **a** scattering cross section, **b** RCS of the uncloaked target, **c** RCS of the cloaked target, **d** polar plot of scattered power along the azimuth plane and **e** effect of incident angle on RCS

describes the scattering cross section of the cloaked (red) and uncloaked targets (black) under plane wave illumination. It is interesting to note that the SCS of the cloaked target shows a significant dip at 1.63 GHz in comparison with the bare metallic cylinder. To study the scattering properties of the two structures, three-dimensional scattered power of the cloaked and uncloaked schemes at 1.63 GHz are studied and the corresponding RCS plots are illustrated in Fig. 2b, c, respectively. The acute scattering from the cylinder target is due to the presence of the non-resonant electric dipole moments and it scatters electromagnetic power equally in the azimuth plane. The maximum RCS of the cloaked target is found to be significantly low in comparison with that of the cylinder. The polar RCS pattern along the azimuth plane illustrated in Fig. 2d also confirms scattering reduction behavior of the structure for normal incidence. Simulation studies have also been performed to find the effect of angle of incidence on RCS of the cloaked cylinder and the results are illustrated in Fig. 2e. It could be seen that RCS is almost independent on the angle of incidence and hence the object is invisible to an observer viewing from various azimuth angles. We have also performed simulation studies by exciting TM polarization in which the electric field is oriented perpendicular to the axis of the cylinder. We have observed that TM polarization could not excite resonance in the proposed structure and hence such studies are omitted here for brevity.

To validate the scattering characteristics of the developed cloak, simulated field distributions in the computational domain are studied at 1.63 GHz in CST Microwave Studio and these results are illustrated in Fig. 3. Figure 3a, b show the top view of the computed magnetic field and Poynting vector distributions across the computational domain. The wave is propagating from the left side of the computational domain to the right side. The uncloaked target perturbs the flow of electromagnetic waves and a shadow is observed behind the target. This means that the bare cylinder scatters incident power and hence one could easily detect its presence from far-field scattering measurements. Figure 3c, d depict the corresponding field distributions for the cloaked target. The inclusion of dogbone metallization around the target smoothly transfers electromagnetic power around the target and a smooth flow of electromagnetic waves around the target is observed. The shadow produced previously is absent in the cloaked target.

To study the reason behind this scattering suppression, multipole scattering theory has been utilized to retrieve the resonant mechanism of the miniaturized structure [25]. Scattered power form the induced multipoles could be calculated by integrating the spatially distributed current distribution

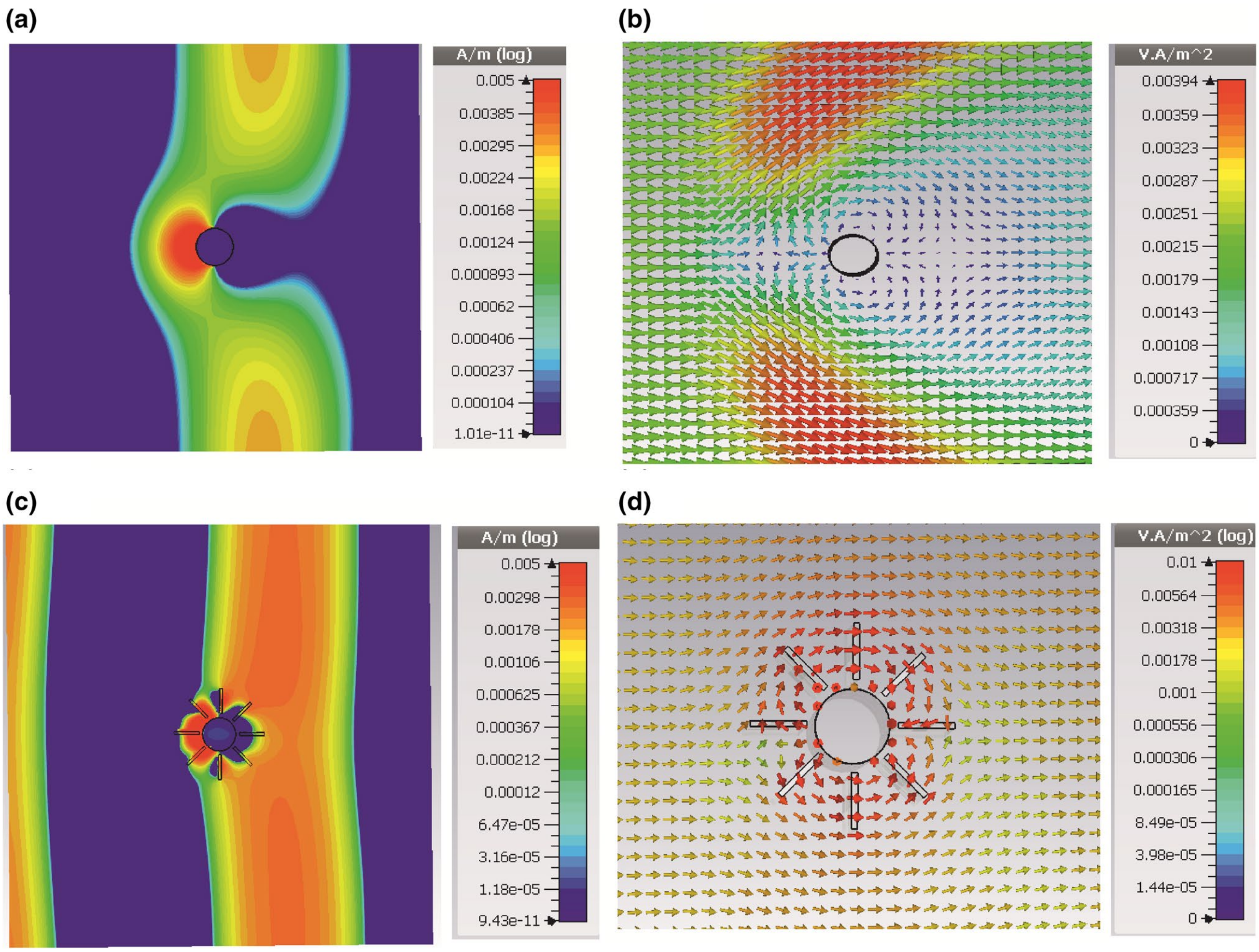

Fig. 3 Results of numerical simulation for the cloaked and uncloaked target at 1.6 GHz **a** magnetic field distribution from the *YZ* plane of the uncloaked target, **b** pointing vector distribution for the uncloaked target, **c** magnetic field distribution of the cloaked target and **d** pointing vector distribution for the cloaked target

over the unit cell. The multi-pole amplitudes can be calculated as

$$P = \frac{1}{i\omega}\int J \mathrm{d}^3 r, \tag{1}$$

$$M = \frac{1}{2c}\int (\vec{r} X J) \mathrm{d}^3 r, \tag{2}$$

$$T = \frac{1}{10c}\int [(\vec{r}.J) - 2r^2 J] \mathrm{d}^3 r, \tag{3}$$

where P, M, and T are the electric, magnetic and toroidal dipole moments, c is the velocity of light in vacuum, $\rightarrow_r$ is the displacement vector from the origin, ω is the angular frequency, and J is the surface current density retrieved from simulations. The total power radiated from different multipole moments can be formulated as

$$I = \frac{2\omega^4}{3c^3}|P|^2 + \frac{2\omega^4}{3c^3}|M|^2 + \frac{2\omega^6}{3c^5}|T|^2 + \cdots . \tag{4}$$

Corresponding radiated powers from the electric (P_y), Magnetic (M_x), and Toroidal (T_y) dipole moments are illustrated in Fig. 4. It is observed that the electric dipole moment is strongly suppressed throughout the entire frequency band. In addition, the magnitude of power scattered by the magnetic dipole moment is of the order greater than 1000 times as compared to that from the electric dipole moment. This peculiar scattering behavior is observed in asymmetric Fano resonance-based scattering cancellation schemes. In an asymmetric Fano interference scheme, the electric and magnetic modes interfere destructively giving rise to a net reduction in scattering cross section. We have also computed the scattering contribution from Toroidal moment T_y and is indicated using blue lines in the graph. In our previous design [24], the presence of toroidal moments at resonance

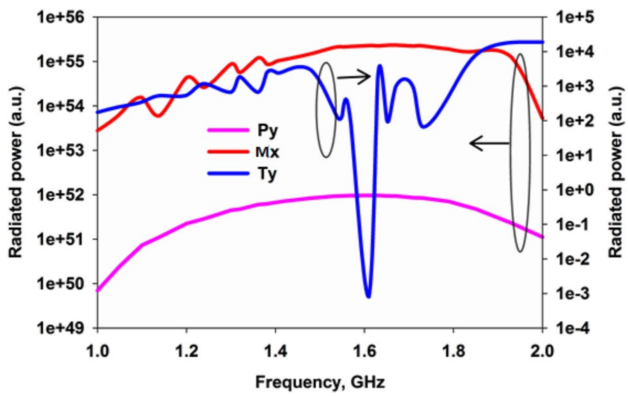

Fig. 4 Radiated power from different multipoles

strongly enhances forward scattering from the composite. But in the present scenario, the toroidal moment shows a significant dip at resonance. This means that excitation of the toroidal moment is significantly weak in comparison with the electric and magnetic dipole moments. This could be said as the destructed toroidal moment and this destructed response suppresses scattering from the structure.

The excitation of Fano-like resonance in the structure is also verified by looking into the surface current and magnetic field distributions excited on the structure for normal incidence as depicted in Fig. 5. The surface currents excited on the target and the vertical dogbone arm are out of phase resulting in a circulating current loop giving rise to the magnetic moment M_φ. One could observe that the surface currents excited on the dogbone elements are in phase and hence the magnetic moments created on them will be in phase as shown in Fig. 5a. As a result, the resultant magnetic field will form confined closed loops in between the metallic target and the dogbone metallization as depicted in Fig. 5b thus creating strong magnetic dipole moments in the composite. Surface currents flowing along the curved C-shaped path and the non-resonant currents on the target constitute the bright radiant electric dipole background mode of the continuum. These anti-symmetric vertical current distributions on the dogbone arm and the target represents the magnetic dipole mode and is called as the dark resonant mode. Hence the resonance dip could be named as the magnetic Fano resonance of the composite. The excitation of magnetic Fano resonance thus modifies the magnetic field distributions in the present frequency band of interest and the excitation of this magnetic resonance destroys the toroidal moment on the structure at the scattering dip.

The advantage of the proposed cloaking technique is the ease of design of the proposed cloaking structure. The design can be easily accomplished by setting the magnetic resonant frequency of the composite. The anti-parallel currents flowing on the dogbone arm and the metallic target can be modeled as a parallel resonant structure and its resonant frequency can be formulated as $F_m = \frac{1}{2\pi\sqrt{LC}}$, where L is the effective inductance offered by the closed path and C is the capacitance of the gaps in between the dogbone arm and the target. So any change in the magnetic resonant frequency will shift the scattering dip accordingly. Two parametric variations have been performed on the structure, one by varying the length L_1 of the dogbone metallization and the second by changing the radial gap S between the dogbone tip and the target and these results are illustrated in Fig. 6. From Fig. 6a, one could observe that the scattering dip is redshifted with an increase in L_1. This is because an increase

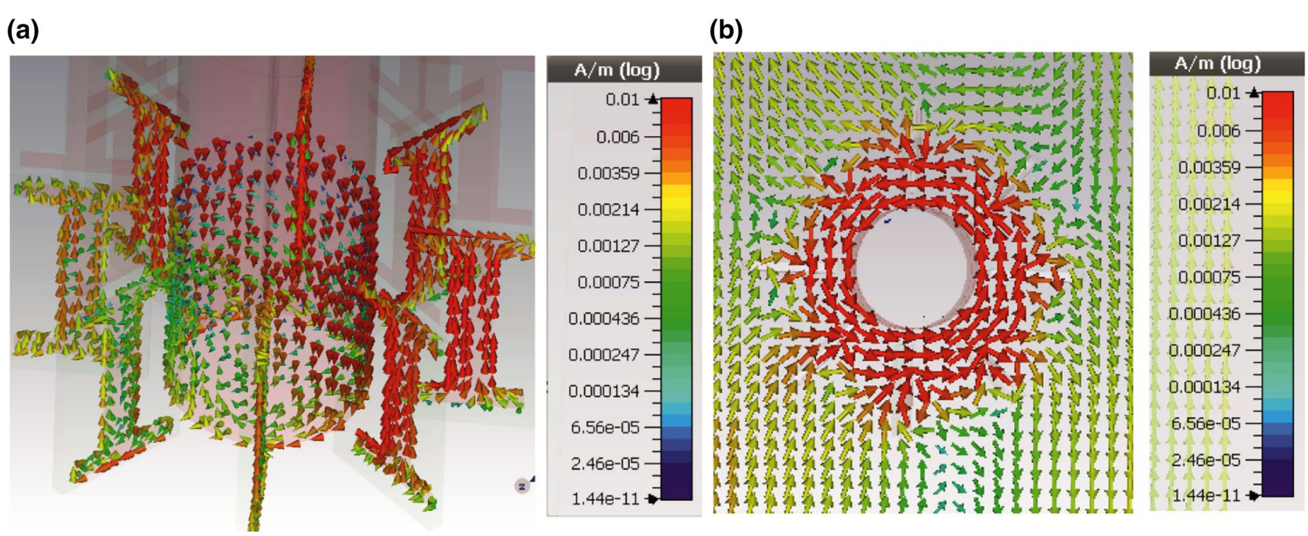

Fig. 5 Computed field distributions on the structure at resonance **a** surface current distribution and **b** top view of magnetic field distribution

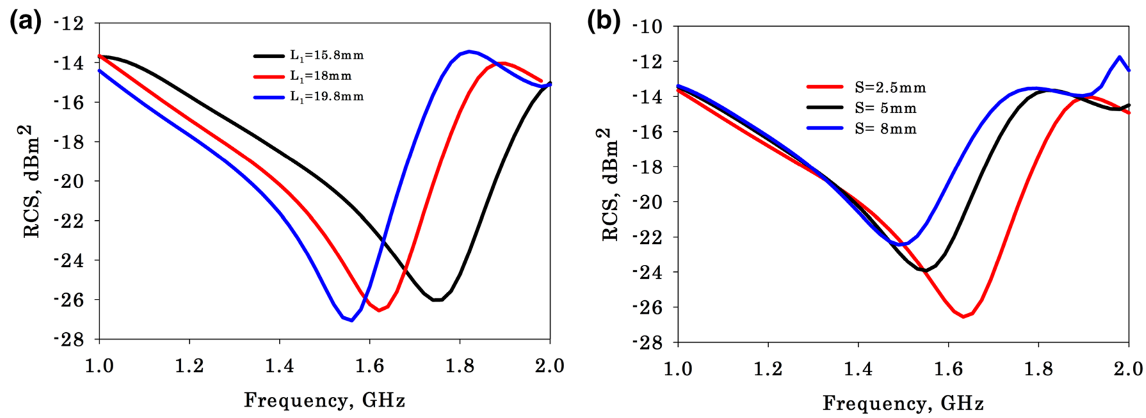

Fig. 6 Results of parametric analysis **a** effect of dogbone length $L1$ and **b** effect of radial distance S on scattering characteristics

in the length of the dogbone metallization increases the effective length of the circular loop resulting in a reduction of the magnetic resonant frequency. The variation in the magnitude of RCS at the resonant dips is found to be negligible in this case. The radial displacement of the dogbone elements also causes a red shift in scattering dip. Here also the effective resonant path is increased because the path length offered by the displacement currents flowing in between the edge of the dogbone element and the target is elongated. But this redshift is accompanied by a reduction in RCS of the structure and this can be accounted by the reduction in magnetic dipole moment in the composite. So for achieving a maximum reduction in scattering power, a strong excitation of magnetic dipole moments on the structure is required.

Monostatic and bistatic scattering measurements are performed on the cloaked target and the results are illustrated in Fig. 7. For measurements, two UWB antennas were utilized, one configured in transmission and the other in reception mode. The antennas were positioned on a rotatable arm turntable assembly with the target at the center. The frequency gated by time (FGT) calibration is performed to select reflection from the metallic target and the corresponding received power is taken as the reference. The target is then replaced by the cloaking structure and is rotated in the azimuth plane using a computer-controlled turntable assembly and the corresponding received power is recorded. Corresponding Monostatic backscattered power is shown in Fig. 7a. It is seen that the backscattered power is significantly reduced as compared to that of the bare metallic target. Bistatic measurements have been performed by rotating the receiving horn antenna around the target with the transmitting antenna held fixed. Corresponding backscattered power is depicted in Fig. 7b. It is seen that a significant reduction in

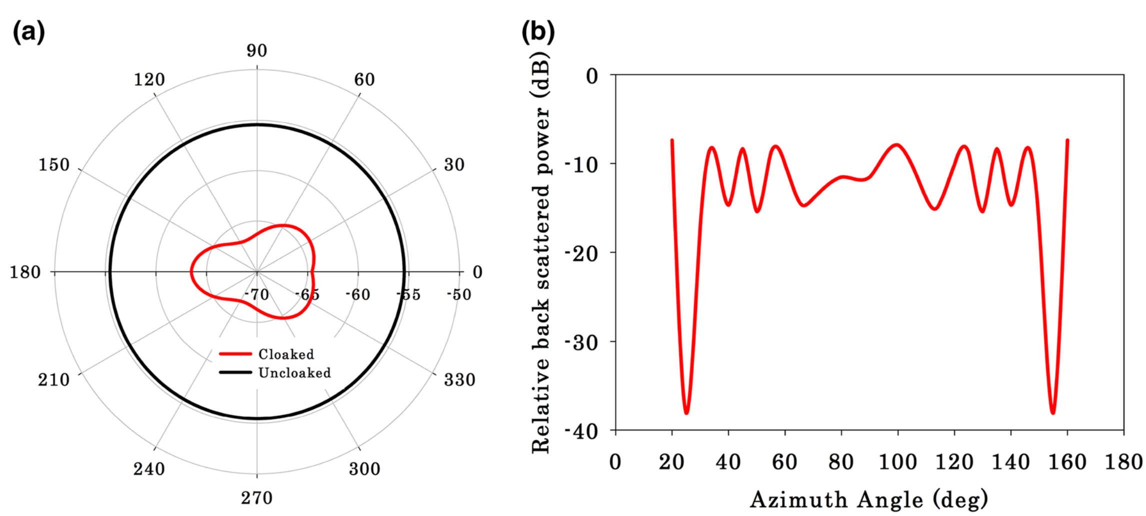

Fig. 7 Backscattering measurements on the fabricated cloak at resonance **a** monostatic backscattered power from the cloaked (red) and uncloaked (black) targets, and **b** bistatic backscattered power from the cloaked target

backscattered is observed within the measurement range. Scattering reduction better than −7.9 dB is observed within the entire measurement range. This implies that the target becomes invisible from backscattering measurements.

3 Conclusions

A Fano-like resonance-based miniaturized cylindrical electromagnetic cloaking scheme is experimentally demonstrated in this paper. Fano-like resonance is created by the coexistence of an electric dipole and magnetic dipole resonance in the composite. Multipolar scattering theory reveals that scattering from the toroidal dipole moment is showing a strong dip at resonance favoring scattering reduction. Full-wave electromagnetic simulations have been performed to verify the operation of the designed cloak in the microwave frequency regime. The simulation results are also validated inside an anechoic chamber using Monostatic and bistatic scattering measurements.

Acknowledgements The authors acknowledge the research funding received from the Science and Engineering Research Board (SERB), Department of Science and Technology for the major research project ECR/2017/002204.

References

1. M. Kerker, D.S. Wang, H. Chew, D.D. Cooke, Does Lorentz-Mie scattering theory for active particles leads to a paradox? Appl. Opt. **19**, 1231 (1980)
2. C.F. Bohren, D.R. Huffman, *Absorption and Scattering of Light by Small Particles* (Wiley, New York, 1983)
3. M. Kerker, D.S. Wang, L. Giles, Electromagnetic scattering by magnetic spheres. J. Opt. Soc. Am. **73**, 765–767 (1983)
4. D. Schurig, J.J. Mock, B.J. Justice, S.A. Cummer, J.B. Pendry, A.F. Starr, D.R. Smith, Metamaterial electromagnetic cloak at microwave frequencies. Science **314**, 977–980 (2006)
5. A. Alù, N. Engheta, Achieving transparency with plasmonic and metamaterial coatings. Phys. Rev. E **72**, 016623 (2005)
6. M.G. Silveirinha, A. Alù, N. Engheta, Parallel-plate metamaterials for cloaking structures. Phys. Rev. E **75**, 036603 (2007)
7. A. Alù, N. Engheta, Cloaking a sensor. Phys. Rev. Lett. **102**, 233901 (2009)
8. A. Alù, Mantle cloak: invisibility induced by a surface. Phys. Rev. B **80**, 245115 (2009)
9. P.Y. Chen, A. Alu, Mantle cloaking using thin patterned metasurfaces. Phys. Rev. B **84**, 205110 (2011)
10. Y.R. Padooru, A.B. Yakovlev, P.Y. Chen, A. Alù, Analytical modeling of conformal mantle cloaks for cylindrical objects using sub-wavelength printed and slotted arrays. J. Appl. Phys. **112**, 034907 (2012)
11. P.Y. Chen, A. Alu, Atomically thin surface cloak using graphene monolayers. ACS Nano **5**, 5855–5863 (2011)
12. U. Fano, Effects of configuration interaction on intensities and phase shifts. Phys. Rev. **124**, 1866–1878 (1961)
13. J. Faist, F. Capasso, C. Sirtori, K.W. West, L.N. Pfeiffer, Controlling the sign of quantum interference by tunneling from quantum wells. Nature **390**, 589–591 (1997)
14. J.A. Fan, K. Bao, C. Wu, J. Bao, R. Bardhan, N.J. Halas, V.N. Manoharan, Fano-like interference in self-assembled plasmonic quadrumer clusters. Nano Lett. **10**(11), 4680–4685 (2010)
15. K.B. Samusev, M.V. Rybin, A.K. Samusev, M.F. Limonov, Invisibility of a finite dielectric cylinder under Fano resonance conditions. Phys. Sol. State **57**, 1991–1996 (2015)
16. B. Luk'yanchuk, R. Paniagua-Domínguez, A.I. Kuznetsov, A.E. Miroshnichenko, Y.S. Kivshar, Suppression of scattering for small dielectric particles: anapole mode and invisibility. Philos. Trans. R. Soc. A **375**, 20160069 (2016)
17. M.V. Rybin, D.S. Filonov, P.A. Belov, Y.S. Kivshar, M.F. Limonov, Switching from visibility to invisibility via Fano resonances: theory and experiment. Nat. Sci. Rep. **5**, 8774 (2015)
18. F. Shafiei, F. Monticone, K.Q. Le, X.X. Liu, T. Hartsfield, A. Alù, X. Li, A subwavelength plasmonic metamolecule exhibiting magnetic-based optical Fano resonance. Nat. Nanotechnol. **8**(2), 95 (2013)
19. B. Hopkins, D.S. Filonov, A.E. Miroshnichenko, F. Monticone, A. Alù, Interplay of magnetic responses in all-dielectric oligomers to realize magnetic Fano resonances. ACS Photonics **2**(6), 724–729 (2015)
20. F. Monticone, A. Alu, The quest for optical magnetism: from splitring resonators to plasmonic nano particles and nanoclusters. J. Mater. Chem. C **2**(43), 9059–9072 (2014)
21. V.P. Sarin, M.P. Jayakrishnan, P.V. Vinesh, C.K. Aanandan, P. Mohanan, K. Vasudevan, An experimental realization of cylindrical cloaking using dogbone metamaterials. Can. J. Phys. **95**, 927–932 (2017)
22. G. Donzelli, A. Vallecchi, F. Capolino, A. Schuchinsky, Metamaterial made of paired planar conductors: particle resonances, phenomena, and properties. Metamaterials **3**, 10–27 (2009)
23. S.V. Pushpakaran, J.M. Purushothama, M. Mani, A. Chandroth, M. Pezholil, V. Kesavath, A metamaterial absorber based high gain directional dipole antenna. Int. J. Microw. Wirel. Tech. **10**, 430–436 (2018)
24. V.P. Sarin, P.V. Vinesh, M. Manoj, C.K. Aanandan, P. Mohanan, K. Vasudevan, Toroidal dipole-induced coherent forward scattering from a miniaturized cloaking structure. Appl. Phys. A **126**, 90 (2020)
25. H. Song, M. Gupta, L. Cong, Y.K. Srivastava, R. Singh, Toroidal and magnetic Fano resonances in planar THz metamaterials. J. Appl. Phys. **112**, 113105 (2017)